

PCCP

Accepted Manuscript



This is an *Accepted Manuscript*, which has been through the Royal Society of Chemistry peer review process and has been accepted for publication.

Accepted Manuscripts are published online shortly after acceptance, before technical editing, formatting and proof reading. Using this free service, authors can make their results available to the community, in citable form, before we publish the edited article. We will replace this *Accepted Manuscript* with the edited and formatted *Advance Article* as soon as it is available.

You can find more information about *Accepted Manuscripts* in the [Information for Authors](#).

Please note that technical editing may introduce minor changes to the text and/or graphics, which may alter content. The journal's standard [Terms & Conditions](#) and the [Ethical guidelines](#) still apply. In no event shall the Royal Society of Chemistry be held responsible for any errors or omissions in this *Accepted Manuscript* or any consequences arising from the use of any information it contains.

Optical Trapping and Raman Spectroscopy of Solid Particles

L. Rkiouak^{1,2}, M.J. Tang^{2,4}, J. Camp¹, J. McGregor³, I. M. Watson⁴, R.A. Cox², M. Kalberer², A. D. Ward^{5*} and F. D. Pope^{6*}

¹Department of Chemical Engineering and Biotechnology, University of Cambridge, Pembroke Street, Cambridge CB2 3RA, UK

²Department of Chemistry, Centre for Atmospheric Sciences, University of Cambridge, Lensfield Road, Cambridge CB2 1EW, UK

³Department of Chemical and Biological Engineering, University of Sheffield, Mappin Street, Sheffield S1 3JD, UK

⁴Department of Earth Sciences, University of Bristol, Wills Memorial Building, Bristol BS8 1RJ, UK

⁵Central Laser Facility, Rutherford Appleton Laboratory, Chilton, Didcot, Oxon OX11 0QX, UK

⁶School of Geography, Earth and Environmental Sciences, University of Birmingham, Edgbaston, Birmingham B15 2TT, UK

* Corresponding authors

1

2 **Abstract**

3 The heterogeneous interactions of gas molecules on solid particles are crucial in many areas of
4 science, engineering and technology. Such interactions play a crucial role in atmospheric chemistry
5 and in heterogeneous catalysis, a key technology in the energy and chemical industries. Investigating
6 heterogeneous interactions upon single levitated particles can provide significant insight into these
7 important processes. Various methodologies exist for levitating micron sized particles including:
8 optical, electrical and acoustic techniques. Prior to this study, the optical levitation of solid micron
9 scale particles has proved difficult to achieve over timescales relevant to the above applications.

10

11 In this work, a new vertically configured counter propagating dual beam optical trap was optimized to
12 levitate a range of solid particles in air. Silica (SiO₂), α -alumina (Al₂O₃), titania (TiO₂) and
13 polystyrene were stably trapped with a high trapping efficiency ($Q = 0.42$). The longest stable
14 trapping experiment was conducted continuously for 24 hours, and there are no obvious constraints on
15 trapping time beyond this period. Therefore, the methodology described in this paper should be of
16 major benefit to various research communities. The strength of the new technique is demonstrated by
17 the simultaneous levitation and spectroscopic interrogation of silica particles by Raman spectroscopy.
18 In particular, the adsorption of water upon silica was investigated under controlled relative humidity

- 1 environments. Furthermore, the collision and coagulation behaviour of silica particles with
- 2 microdroplets of sulphuric acid was followed using both optical imaging and Raman spectroscopy.

1 1 Introduction

2 The adsorption of molecules onto solid particle surfaces plays an important role in many fields of
3 science, technology and engineering. For example it is of key significance in atmospheric chemistry,
4 heterogeneous catalysis, surface science and sensor development.

5
6 In the atmosphere, mineral dust aerosol is the most abundant aerosol type by mass over global land
7 surfaces¹. It is formed by wind erosion of desert regions which cover approximately one third of the
8 global land surface. Individual mineral dust aerosol is typically micron sized and as an ensemble it
9 provides a large surface area for heterogeneous reactions. These reactions are important for
10 controlling the tropospheric concentrations of trace gases such as N_2O_5 , H_2O_2 and HO_2 ²⁻⁴. In
11 addition to naturally occurring sources of solid minerals, it has recently been proposed that the
12 injection of mineral aerosols into the stratosphere could be used as a solar radiation management
13 geoengineering scheme^{2,5}, and one of the motivations of this work was the lack of methodologies to
14 study the reactivity of these particle types.

15
16 Elsewhere, catalytic processes underpin the energy and manufacturing industries; the interaction of
17 reactants with solid catalysts is a key step in the production of fuels, polymers, drugs and other
18 chemicals. In all of these fields metal-oxides play a crucial role. Silica (SiO_2), alumina (Al_2O_3) and
19 titania (TiO_2) are major components of naturally occurring mineral dust aerosol, and are also common
20 support-materials in heterogeneous catalysis, in addition to having catalytic properties in their own
21 right^{6,7}.

22
23 Single particle levitation techniques allow for the investigation of adsorbate-adsorbent (gas-solid
24 surface) interactions. Various levitation techniques are possible which rely on either optical forces
25 (e.g. King *et al.*)⁸, electrodynamic forces (e.g. Pope *et al.*)⁹, or acoustic forces (e.g. Priego-Capote)¹⁰
26 to offset the effects of gravity. Each technique has distinct advantages and disadvantages as reviewed
27 by Krieger, Marcolli and Reid¹¹. For solid particles, the use of an electrodynamic balance (EDB) and
28 acoustic traps are typically more convenient because these traps place little constraint on particle
29 shape, whereas optical traps require a degree of spherical symmetry¹². It should be noted that optical
30 trapping within liquid media has allowed for the manipulation of a variety of non-spherical particle
31 shapes including cylinders, spheroids, wire and propeller shapes¹³⁻¹⁷. However, all of these shapes
32 contain some symmetry through which the optical trap can function. Within aerosol systems (solid or
33 liquid in gas), the low density of the surrounding gas media produces little damping¹⁸, thereby
34 increasing experimental difficulty, and hence the majority of studies into the optical trapping of
35 aerosols involve levitating perfect spheres. Exceptions include the trapping of spherical droplets
36 which are then physically or chemically processed to form imperfect spheres, for example Taji *et al.*

1 studied supercooled spherical droplets which formed ice crystals¹⁹. The major disadvantage of the
2 electrodynamic balance approach however is the requirement of the particles to be charged which can
3 lead to perturbations in particle microphysics and chemistry (e.g. Nielsen *et al.*)²⁰. Acoustic traps
4 typically require larger particle sizes compared to optical and electrodynamic traps, and can be
5 unstable due to acoustic streaming²¹. When optical levitation can be utilized it offers excellent
6 prospects for simultaneous trapping and spectroscopic interrogation (e.g. Ward *et al.*)⁸ because both
7 the trapping and spectroscopy light sources can be directed through the same optics thus ensuring
8 optimal alignment.

9
10 Since the first experimental demonstration of optical forces by Ashkin, levitation techniques have
11 become popular^{22–24} and in particular optical tweezers have attracted much attention.^{8,25,26} Most optical
12 trapping of aerosol particles has been performed on particles that are liquid²⁷ or amorphous in state.²⁸
13 However, there have been several previous studies investigating the optical levitation of solid
14 particles. Arita *et al.* manipulated birefringent particles within optical tweezers reporting data
15 accumulated over a timescale of seconds²⁹. Summers *et al.*³⁰ demonstrated the trapping of solid silica
16 particles on the order of minutes using optical tweezers. In a study by Hoffman *et al.*³¹ the maximum
17 levitation time was dependent upon the composition of the particles. Elsewhere, Omori *et al.*²⁵ trapped
18 particles for more than 30 minutes. The most detailed studies are from Li *et al.*^{32–34} where a horizontal
19 counter-propagating dual-beam (CPDB) trap was used to follow Brownian motion of silica beads
20 trapped for many hours. Whilst previous studies have demonstrated the trapping of solid particles
21 over various timescales, no previous studies have integrated the trapping of solid microspheres with
22 spectroscopic techniques to probe the heterogeneous chemistry of these important systems.

23
24 The concept of using CPDB traps dates from the earliest studies of laser tweezers²³ and has been
25 refined³⁵ by using low numerical aperture (NA) objective lenses to improve the focussing
26 characteristics and alignment accuracy of the laser beams thus increasing optical trapping efficiency.
27 As detailed by Kraikivski *et al.*, the efficient optical trapping of spherical particles, in liquid water,
28 using counter-propagating laser beams is achieved when the particle radius and the beam waist of the
29 focussed laser beam are of similar size³⁶. Fulfilling this condition generates the maximum radiation
30 pressure from each of the focussed laser beams for a given laser power. The stability of counter-
31 propagating traps for small particles is reported to require a small and positive separation between the
32 foci of the two counter propagating beams. As an example, stable trapping of a 4 μm diameter
33 polystyrene bead in water was achieved with a focal separation of $6 \pm 3 \mu\text{m}$ ³⁶.

34
35 In this paper we describe an experimental strategy with which to form a robust optical levitation trap
36 for solid micron sized solid particles. The approach does not require feedback control and hence can
37 be set up in a relatively straight forward manner. The stable trapping of SiO_2 , Al_2O_3 , TiO_2 and

1 polystyrene (which also has applications as a catalyst support³⁷) microsphere particles is
2 demonstrated. We combine this optical trapping with Raman spectroscopy; a combination which
3 allows the determination of chemical and physical characteristics on a single-particle basis.³⁸ The
4 strength of the technique for studying solid particles is shown through observations, via Raman
5 spectroscopy, of the adsorption of water on silica particles and the coagulation of sulphuric acid
6 droplets with silica particles.

7

2 Experimental

2.1 Sample preparation

Solid particles were delivered to a small trapping cell, of aluminium construction, with approximate dimensions $10 \times 2 \times 1$ cm. Windows made from borosilicate cover slips allowed the passage of the laser beams through the cell (see Figure 1a). The particles were generated using an atomizer (Topas Aerosol Generator ATM 220) filled with a 2.5 % w/w suspension of the solid particles in water. Nitrogen (N_2) was used as the carrier gas, at a flow rate of 10 ml min^{-1} , and was generated from the boil-off from a liquid nitrogen tank. The gas flow into and out of the trapping cell is via two parallel ports attached to the same face of the cell. This generates slow flow conditions at the position of the trapped particle, thereby reducing the external forces on the particle. All measurements were performed at ambient temperature (293 K).

The following solid particles were used in the trapping experiments: silica (Whitehouse Scientific, MSS002, nominal diameter = $2 \mu\text{m}$), α -alumina (Corpuscular Inc., C-ALU-2.0 #130214-10, nominal diameter = $2 \mu\text{m}$), amorphous titania (Corpuscular Inc., C-TIO-2.0 #220214-10, nominal diameter = $2 \mu\text{m}$) and polystyrene (Interfacial Dynamics, Latex Particles #S37500, nominal diameter = $2 \mu\text{m}$). The absolute size distribution of the solid particles was measured using scanning electron microscopy (FEG Digital Scanning Microscope, 1530 VP Gemini LEO, which was equipped with an EDAX detector, EDS Sapphire) as shown in Figure 2. The samples were fixed with double-sided conductive adhesive on cups of 5 mm diameter (Agar Scientific). The software program Image J (version 1.47) was used for image processing and analysis. The measured particles have a narrow size distribution, with average particle diameter and standard deviation provided in Table 1.

For the relative humidity (RH) dependent measurements, the RH of the cell was controlled by varying the ratio of dry and water saturated N_2 gas flows that were combined and passed into the cell as shown in Figure 1(a). The water saturated N_2 gas flow was generated by flowing dry N_2 through a water bubbler. The cell RH was measured using a Sensirion SHT-75 RH sensor, placed at the entrance of the trapping cell, with a stated accuracy of $\pm 1.8\%$. For the sulphuric acid coagulation experiments, an ultrasonic nebuliser (Schill Mobil Aerosonic 3060) containing 2M sulphuric acid solution (VWR, technical grade) generated a sulphuric acid mist with droplet sizes in the approximate range: $1 - 7 \mu\text{m}$.

1 2.2 Counter-propagating dual-beam optical trap

2 A simplified representation of the optical system is shown in Figure 1(b). The particles were trapped
3 using an Nd:Yag laser (Ventus, Laser Quantum) operating at 1064 nm. The typical laser beam
4 powers required for stable trapping were 15 mW through the top objective and 10 mW through the
5 lower objective. The asymmetric power balance was required to force the particle into the optical
6 focus plane of the lower objective thereby allowing focused images to be acquired. The Nd:Yag
7 beam is passed through a beam splitter (Oz Optics) to obtain two separate fibre-coupled beams. Both
8 beams are then expanded and collimated so that they slightly overfill the back apertures of the
9 objective lenses. Dichroic mirrors (CVI Melles Griot) reflect the laser beams but allow transmission
10 of illumination light and the Raman signals. The LED illumination (Comar Optics) is filtered to
11 prevent interference with the Raman signal. The trapped particle is imaged from two directions: first
12 using the trapping objective lenses as a conventional microscope with the top objective acting as a
13 condenser. The second image is a horizontal view from the side of the sample holder and is taken with
14 a Mitutoyo Plan Apo $\times 20$ long working distance objective.

15
16 As none of the investigated particles possess significant absorbance coefficients at the trapping laser
17 wavelength (1064 nm)³⁹⁻⁴⁶, we expect negligible heating of the particle due to absorbance of the
18 trapping laser beams.

19
20 To achieve stable trapping, for extended periods of time, the waist of the focused laser beam is made
21 comparable to the particle radius as described previously in the liquid phase work of Kraikivski *et*
22 *al.*³⁶. In the present study the particle radii are typically 1.0 μm and the calculated beam waist from
23 the Mitutoyo $\times 50$ objective (NA 0.42) is 1.4 μm , the focal separation, between the foci of the two
24 counter propagating beams, was typically 10 ± 1 microns for the majority of particles studied. The
25 separation was controlled using a differential micrometer for z-axis movement of the upper objective
26 lens. Separation was determined using the image of the laser focal spot of the lower objective lens as a
27 reference. Imaging the focal spot enabled x, y and z alignment of the focussed beams. The optical
28 configuration described in this paper, resulted in a robust 3-dimensional trap which requires no further
29 control systems, such as force feedback⁴⁷, to retain the particle in air.

31 2.2 Raman spectroscopy setup

32 A 514.5 nm Ar-ion laser (Innova 300C, Coherent) was focused on the particle to generate Raman
33 scattered light. The 514.5 nm laser used for Raman excitation was used at typical powers of ~ 9 mW.
34 It should be noted that Hunt *et al.*⁴⁸ demonstrated that low 514.5 nm laser powers (< 16 mW) did not
35 cause significant temperature changes within a single-beam gradient trapped sulphuric acid droplet.
36 The molar absorption coefficient of sulphuric acid^{49,50} is greater than that of all the particles

1 investigated, at 514.5 nm, and hence we expect no significant heating effect to be present in the
2 approach used in this study⁵¹. The Ar-ion passes through beam expansion optics before combination
3 with the 1064 nm laser beam using a dichroic mirror. The backscattered Raman signal from the
4 trapped micro-particle is collimated by the objective lens and passes back along the same optical
5 pathway. The signal is transmitted through a dichroic Razor Edge mirror (Semrock) and through a
6 514.5 nm edge filter (Semrock) to remove Rayleigh scattering. The light is finally focused on a
7 spectrograph (SpectraPro 2500i, 1200 groove blazed at 500 nm) and imaged onto a CCD camera
8 (Princeton Instruments, Spec10). Raman signals were collected with integration times of ~60 s.
9 Wavelength calibration was achieved by recording the Raman spectrum of bulk toluene (Sigma
10 Aldrich Spectrophotometric grade) which is well characterised^{52–55}.

1 3 Results and Discussion

2 First, we demonstrate the ability of the CPDB to stably trap solid particles over long time periods, of
 3 up to one day. Then using this technique we characterise the Raman signal observed from SiO₂, TiO₂,
 4 Al₂O₃ and polystyrene microspheres. Finally we report two in-depth spectroscopic studies upon
 5 levitated SiO₂ particles: (i) the absorption of water vapour; and (ii) the coagulation with sulphuric acid
 6 mist particles.

7 3.1 Stable trapping of solid particles

8 Stable trapping of TiO₂, SiO₂, Al₂O₃ and polystyrene particles was routinely achieved using the
 9 CPDB trap for extended periods of time. The longest time period that a particle (SiO₂ particle in a dry
 10 air environment) was trapped for was 24 hours, after which time the particle was deliberately
 11 dislodged. We are confident that the technique described in this paper places no constraints on
 12 trapping time, for the particle compositions investigated.

13

14 The efficiency of the optical trap was evaluated by measuring the minimum laser power required to
 15 keep the particle in the trap. From this, the vertical efficiency of the trap can be calculated. The
 16 trapping efficiency Q is defined by the expression $Q = Fc/nP$, where F is the force exerted on the
 17 particle, P is the power of the laser beam, n is the refractive index of the surrounding medium, and c is
 18 the speed of light in free space.⁵⁶ The maximum value of Q is 1 and indicates a completely efficient
 19 trap with respect to using all the available momentum from the laser radiation. The force exerted on
 20 the particle is calculated by taking the difference between the gravitational and the radiation power P_1
 21 (the upward beam) and P_2 (the downward beam) as shown in Equation E1:

22

$$23 \quad Q n \frac{(P_1 - P_2)}{c} = \frac{4}{3} \pi r^3 \rho g \quad \text{E1}$$

24

25 where r is the radius of the particle, g is the gravitational force and ρ is the density of the particle.

26

27 In our measurements to determine the minimum laser power required for trapping in air both the laser
 28 powers and focal separation were systematically varied. The minimum laser powers were recorded
 29 when the focal separation was of 1 ± 1 micron separation. Thus, the configuration we use differs as
 30 compared to the majority of other set-ups, including the work of Kraikivski et al.³⁶, in that the
 31 optimum focal separation of the counter-propagating trap (1 μm) is of similar dimension to the beam
 32 waist (1.4 μm) and particle size (1.0 μm). For α -alumina particles (as a representative example) a
 33 minimum upward beam of 0.60 ± 0.01 mW and a downward beam of 0.50 ± 0.01 mW were sufficient
 34 to trap a particle ($\rho = 3720$ kg m⁻³) of 2.2 ± 0.02 μm diameter. Using Equation E1, a trapping

1 efficiency of 0.42 ± 0.02 is obtained. This value compares to the reported values of 0.2 by Summers
2 *et al.*⁵⁷ and 0.01 by Omori *et al.*,²⁵ both of which were measured for silica particles.

3
4 It should be noted that trapping stability is not the same thing as trapping efficiency. In our optical set
5 up the optimum trapping efficiency was achieved at a focal separation of $\sim 1 \mu\text{m}$. However, the
6 alignment of the focussed laser beams was difficult to maintain over long periods due to constraints of
7 the laboratory environment. The best long term stability was realised with a focal separation of ~ 10
8 μm . At this separation small changes in alignment were found not to be critical to particle trapping.

9 10 **3.2 Raman Signatures of the pure particles**

11 The Raman spectra of the four investigated particles (SiO_2 , TiO_2 , $\alpha\text{-Al}_2\text{O}_3$ and polystyrene) within the
12 optical trap are shown in Figure 3. The spectra shown are background subtracted, the background
13 being acquired under identical conditions in the absence of a trapped particle. No other processing of
14 the data was carried out.

15
16 The Raman spectrum of a trapped SiO_2 particle, as shown in Figure 3(a), exhibits peaks at 390, 490,
17 795, 972 and 1460 cm^{-1} assigned to Si–O–Si bonds^{39,40}. The band at 1460 cm^{-1} is associated with
18 Si–O stretching vibrations. The bands at 795 and 972 cm^{-1} are attributed to the symmetric stretching of
19 Si–O–Si, while the bands at 390 and 490 cm^{-1} are associated with oxygen atom bending in the
20 Si–O–Si vibration. Amorphous TiO_2 (Figure 3(b)) exhibits bands at 484 and 680 cm^{-1} assigned to
21 Ti–O bonds and, while the bands at 317 and 250 cm^{-1} are assigned to O–O interactions^{41,42}.
22 Additionally, the spectrum also shows sharp peaks at 153 and 639 cm^{-1} which are known to be
23 characteristic of the anatase phase of TiO_2 ^{41,42}. This indicates the presence of some crystalline material
24 in the sample which suggests that the amorphous titania contains a proportion of anatase structure⁴³.
25 Figure 3(c) shows the Raman spectrum of trapped $\alpha\text{-Al}_2\text{O}_3$. A broad peak at 420 cm^{-1} is observed
26 along with smaller peaks at 585, 796 and 976 cm^{-1} . The first three peaks correspond to Al–O–Al
27 vibrations⁴⁴, while the latter peak corresponds to Al–OH vibrational modes, indicative of the presence
28 of hydroxyl groups on the alumina surface which could be due to water present in our system.⁴⁵
29 Finally, the spectrum of trapped polystyrene is shown in Figure 3(d) with peaks at 2839 and 2901 cm^{-1}
30 from the methylene stretches. The in and out-of-plane C–H bends of the aromatic ring give rise to the
31 intense peaks at 1002 and 1030 cm^{-1} . The aromatic ring breathing modes appear at 1555 cm^{-1} while
32 the peak at 3069 cm^{-1} corresponds to aromatic C–H stretches. This is consistent with previous reported
33 Raman spectra of this material.⁴⁶

34 **3.3 Relative humidity dependent adsorption of water onto silica particles**

35 Individual SiO_2 particles were trapped, as described in section 3.1, and exposed to a humidified
36 nitrogen flow as described in section 2.1. The flow ratio of dry and H_2O -saturated nitrogen was

1 adjusted to achieve a range of RH between 40 – 80 %. Water is an important adsorbate in many
2 industrial applications, and within the troposphere the RH varies widely. Increasing the relative
3 humidity inside the trapping chamber, from an initial value of ~43 % to a maximum of ~75 % was
4 found to increase the Raman peak intensities associated with the trapped SiO₂ particle at 640 and
5 1805 cm⁻¹, as shown in Figure 4(a). The integration of the peak at 1805 cm⁻¹ is shown in Figure 4(b)
6 as a function of RH.

7
8 The broadness of the Raman band centred at 1805 cm⁻¹ indicates other contributions to the known
9 peak of H-O-H bending vibration which is usually centred at 1600 cm⁻¹. In fact, (Si)O-H vibrational
10 modes of differing hydrogen-bond strength are known to appear around 1800 cm⁻¹. These bands
11 increase in intensity at higher RH due to interactions of water with the hydrophilic SiO₂ surface^{40,58}.
12 The surface silica network of such a highly hydrated solid surface gives rise to peaks that differ from
13 peaks of bulk silica^{39,59-61}. This hypothesis is supported by an increase in the intensity of the peak at
14 640 cm⁻¹, *i.e.* the Si-O-Si symmetric stretch. Those results provide a clear indication of the changes
15 occurring on the particle surface as a result of exposure to and adsorption of H₂O. These changes in
16 particle composition are likely to affect particle reactivity with trace gas species.

17

18 **3.4 Coagulation of silica particles with sulphuric acid particles**

19 Sulphuric acid is a key component of atmospheric aerosols. For example stratospheric ozone
20 chemistry is strongly influenced by the presence of sulphuric acid particles which provide a surface
21 for the chlorine activation responsible for ozone depletion events⁶². The partitioning of sulphuric acid
22 aerosol into sulphate and bisulphate ions, and hence the overall particle composition, depends upon
23 the relative humidity and temperature of the environment local to the particle. Partitioning and
24 composition are also likely to be dependent on the interaction of the sulphate with the other aerosol
25 constituents such as mineral species. Within industrial applications, the interaction of sulphuric acid
26 and metal oxides plays an important role in many catalytic processes where sulphuric acid is a reactant
27 or acts as a sulphonating agent, for example in the preparation of sulphated zirconia or silica
28 catalysts^{63,64}.

29

30 The interaction of sulphuric acid droplets with trapped SiO₂ particles has been investigated as a
31 function of exposure time. The size of the trapped SiO₂ particles are observed to incrementally
32 increase as they are exposed to, and coagulate with, sulphuric acid mist droplets. This is exemplified
33 in Figure 5 which shows an initially pure SiO₂ particle, with an initial diameter of 2.3 μm; grow in
34 diameter as sulphuric acid droplets coagulate with it, to a final size of 4.1 μm after 7 minutes. The
35 images were obtained on the CCD camera and analysed using the Image J program. This data clearly

1 demonstrates the ability to retain a solid particle, within an optical trap, over extended time periods
2 whilst colliding, and coalescing the particle with liquid-droplets (in this case sulphuric acid).

3
4 Raman spectroscopy is ideally suited to provide evidence and quantification of the ionic speciation of
5 sulphuric acid between sulphate (SO_4^{2-}) and bisulphate (HSO_4^-) ions (as shown in reaction R1)^{49,65}.



8
9 The vibrational modes of the sulphate ion (SO_4^{2-}) and the bisulphate ion (HSO_4^-) are well
10 characterised in the literature.^{49,50} The presence of SO_4^{2-} gives rise to peaks at 1120, 980, 610 and
11 450 cm^{-1} , while HSO_4^- yields peaks at 1192, 1110, 1047, 885, 592 and 425 cm^{-1} . In most cases the
12 sulphate and bisulphate ion peaks overlap and hence it is necessary to deconvolute the respective
13 contributions from each ion.⁴⁸ The exceptions are the bands at 979 (SO_4^{2-}), and 1042 cm^{-1} (HSO_4^-).
14 These peaks can therefore be considered as unambiguous references for those ions.⁶⁵ The speciation
15 of sulphuric acid, into sulphate and bisulphate ions, and the equilibrium between the different species
16 is highly dependent upon the pH of the particle. Consequently it is dependent upon the water content
17 of the droplet which is thermodynamically controlled by the relative humidity.³⁶

18
19 Raman spectroscopy is utilized to interrogate the $\text{SiO}_2\text{-H}_2\text{SO}_4$ system. In particular we investigate the
20 speciation of sulphuric acid upon the surface of SiO_2 particles. Figure 6(a) shows the Raman spectra
21 of a pure sulphuric acid droplet and a pure SiO_2 particle, both recorded within the optical trap. Within
22 the sulphuric acid system peaks are clearly identifiable at: 430, 594, 902, 979, 1042 and 1192 cm^{-1} .

23
24 To conduct a fully quantitative analysis of the relative concentrations of the sulphate and bisulphate
25 species from the integrated band intensities, I , it is necessary to obtain the molal scattering coefficient,
26 J .⁶⁷ Within this study the molal scattering coefficients were not determined due to time constraints,
27 instead a calibration factor, f , defined as the ratio of the integrated area of the sulphate ion peak (at
28 979 cm^{-1}) to that of the bisulphate ion peak (at 1042 cm^{-1}) is used to obtain relative concentration
29 values. A calibration point is obtained from the band intensities obtained from a trapped sulphuric
30 acid droplet that was caught immediately after nebulization from a 2 M stock solution (as shown in
31 Figure 6a).⁶⁷ The 2 M calibration point was repeated twice and the ratio of the peak areas was found
32 to be constant within 1σ statistical error. It is assumed that the sulphate partitioning within this droplet
33 is the same as the 2 M stock solution which is well characterised.

34
35 Figure 6(b) provides consecutive Raman spectra of the trapped SiO_2 particle, as a function of time,
36 before, during and after exposure to a burst of sulphuric acid mist droplets. Sulphate and bisulphate
37 ion peaks at 428, 596, 902, 988 and 1042 cm^{-1} are first observed after ~9 minutes, coincident with the

1 onset of sulphuric acid flow. The sulphuric acid nebuliser injection time only lasted for approximately
2 50 s. However this burst results in a continual presence of sulphuric acid droplets within the trapping
3 cell for several minutes due to the slow flow conditions. The exposure of the trapped SiO₂ particle to
4 sulphuric acid droplets leads to a continuous increase in the intensity of the sulphate bands. A blue
5 shift of the sulphate ion peak at 988 cm⁻¹ is observed, compared to the 978 cm⁻¹ of the pure droplets
6 (see Figure 6a). This is likely explained by a change in the sulphate vibrational frequency due to
7 additional absorbate-absorbent interactions not present in the bulk liquid state.⁶⁸ Conversely, no blue
8 shift is observed for the bisulphate ion peak at 1042 cm⁻¹.

9
10 The variation in the total concentration of the sum of sulphate and bisulphate ions, quantified by
11 adding the concentrations of the sulphate to the concentration of the bisulphate using the area of their
12 respective peaks and the calibration factor, is shown Figure 7. The degree of dissociation, α , of the
13 bisulphate ion can be calculated via equation E2, and the temporal variation of α is also shown in
14 Figure 7. It should be noted again that both the concentration and the degree of dissociation are only
15 approximate because the molal scattering coefficients are not known.

$$16 \quad \alpha = \frac{[SO_4^{2-}]}{[SO_4^{2-}] + [HSO_4^-]} \quad E2$$

17
18
19 It can be observed that the total concentration of all three sulphate species increases linearly from 9
20 minutes when sulphuric acid droplets are introduced into the trapping cell until the measurement ends
21 at 18 minutes. In contrast the degree of dissociation increases for only the first 5 minutes of sulphuric
22 acid exposure and then stabilizes at a value of ~0.2. The degree of dissociation is dependent on both
23 the relative humidity and the temperature, therefore the changes in dissociation observed in Figure 7
24 are likely due to variations in RH within the environmental cell. The RH within the environmental
25 chamber during nebulisation will be high since the water vapour activity would be approximately
26 equal to the water activity of the 2M sulphuric acid. This corresponds to a relative humidity of ~90%,
27 as predicted by the E-AIM model⁶⁹. Subsequent to nebulisation, the chamber RH will slowly
28 decrease. An increase in the degree of dissociation of sulphuric acid is predicted as the RH decreases
29 from ~90% to ~80%; below ~80% the degree of dissociation reduces with RH^{69,65,49}. The ability to
30 observe the chemical composition of a particle will allow future work to track detailed reaction
31 kinetics on a single particle level.

4 Conclusions

This study provides a methodology for trapping micron sized solid spherical particles over an extended time period. Trapping times have only been demonstrated to an upper limit of 24 hours, but there is no apparent reason why longer times could not be achieved if desired. High trap stability is achieved using a counter propagating beam optical trap with a measured Q-factor of 0.42. This stable particle levitation can then be combined with Raman spectroscopy to quantitatively study adsorbate-adsorbent interactions on an individual particle basis. This study represents the first application of this technique to a range of solid oxide particles, as well as polystyrene microspheres, and we have demonstrated the significant potential of this approach in fields as diverse as atmospheric science and catalysis. Specifically we have shown the technique can be used for: materials characterisation, water adsorption measurement, surface hydroxylation detection and the characterisation of the partitioning of sulphuric acid, into its sulphate and bisulphate ions, upon interaction with mineral surfaces. This study therefore shows the feasibility and advantages of following heterogeneous reactions on a single-particle scale using optical traps and Raman spectroscopy in a variety of scientific and engineering applications.

Acknowledgements

The support of EPSRC (grant number EP/I01473X/1) is gratefully acknowledged as is linked access to the STFC Central Laser Facility based in the Research Complex at Harwell. The anonymous referees are thanked for their time and effort spent in improving this manuscript.

1 **Table 1:** Mean diameter and standard deviation obtained from the SEM images (Figure 2). Image
2 processing achieved with Image J software.

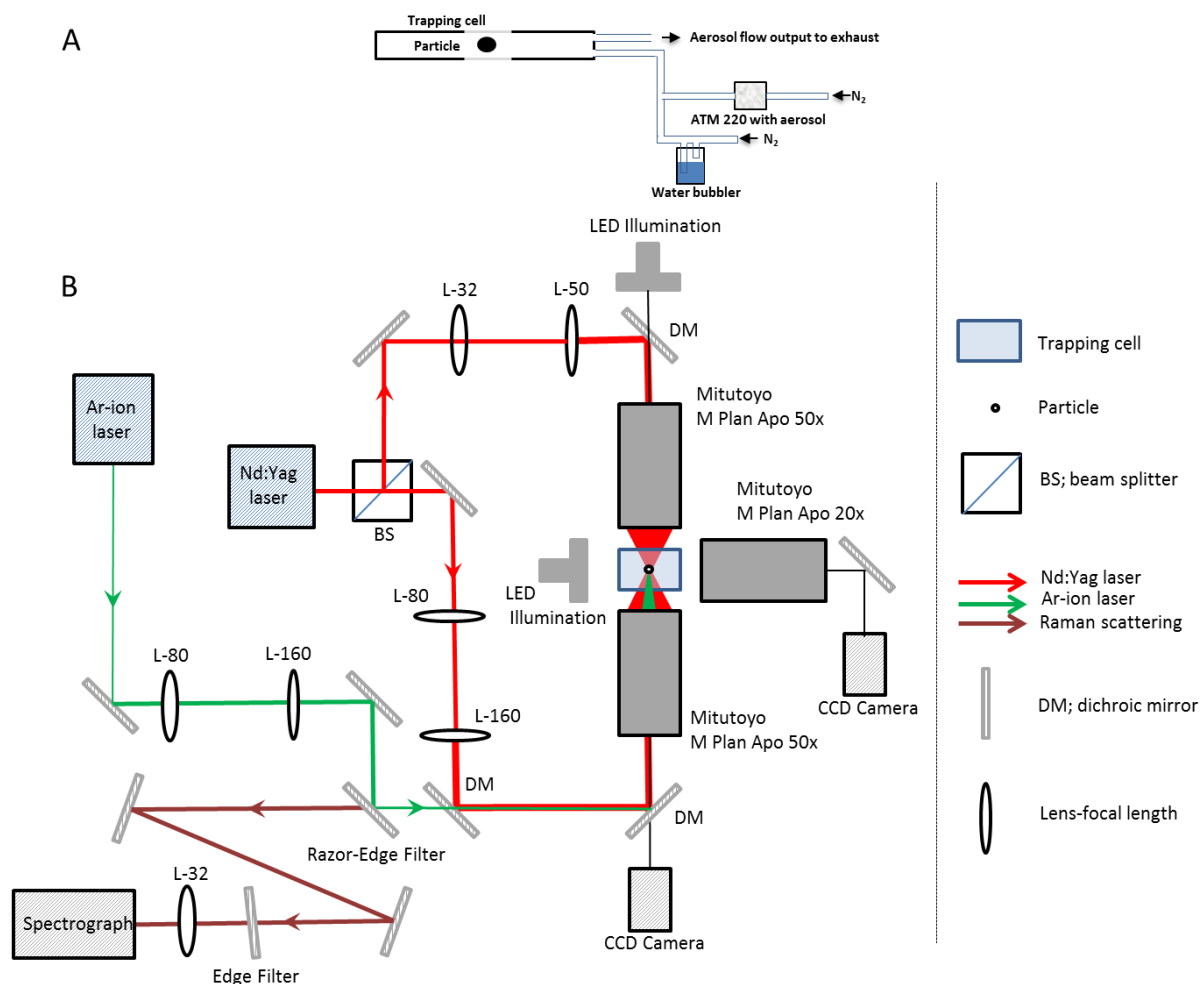
3

Particle Composition	Diameter / μm	Standard Deviation / μm
Silica	1.7	0.3
Titania	2.1	0.4
α -Alumina	2.2	0.2
Polystyrene	2.1	0.1

4

1 **Figures**

2 **Figure 1.** Experimental Setup. Diagram (a) Schematic diagram of the overall experimental apparatus
 3 including: particle generation, humidity control, and trapping cell. Diagram (b) Schematic diagram of
 4 the optical setup of the counter-propagating dual-beam optical trap combined with Raman
 5 spectroscopy. The Mitutoyo $\times 50$ objective lenses are mounted vertically. DM = dichroic mirror, L-
 6 50 = 50 mm focal length lens, BS = beam splitter.



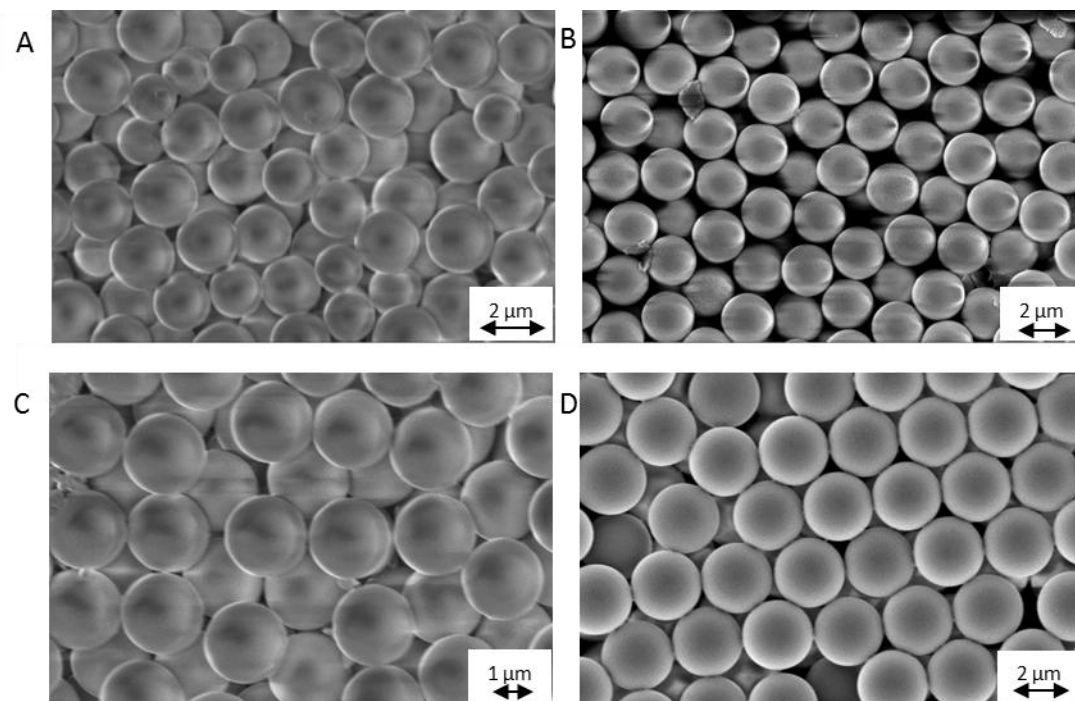
7

1

2

3

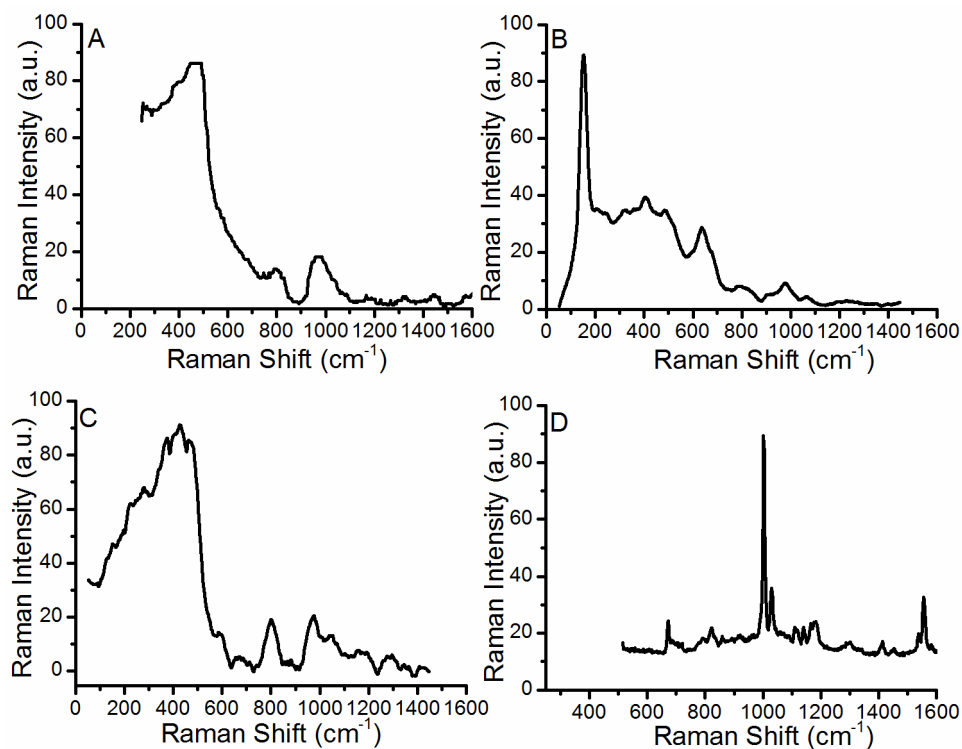
4 **Figure 2:** Scanning electron microscope (SEM) images of (a) silica, (b) titania, (c) α -alumina and (d)
5 polystyrene microspheres which were used in the optical trapping experiments. SEM measurements
6 performed using a FEG Digital Scanning Microscope equipped with an EDAX detector.



7

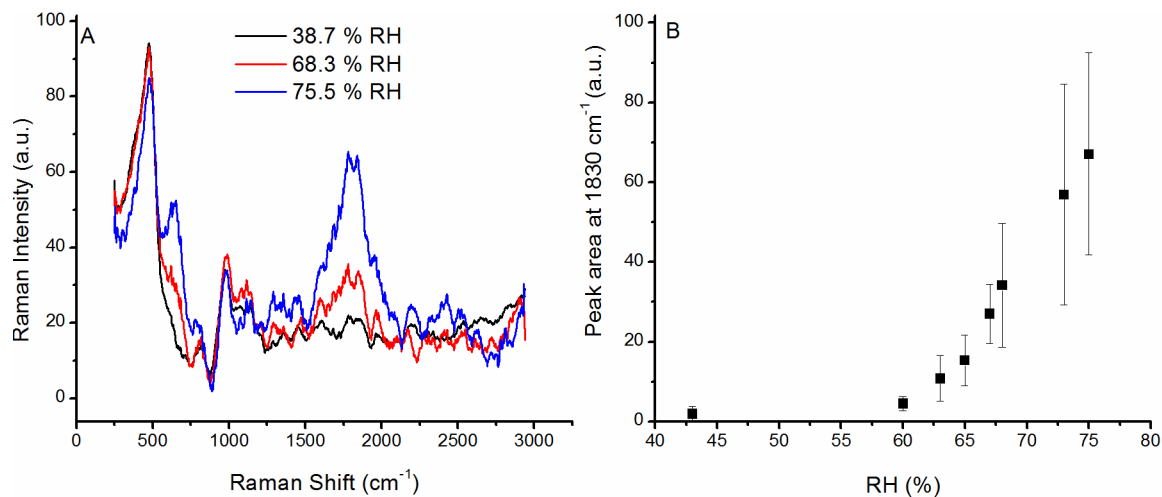
8

- 1 **Figure 3:** Raman spectra of trapped particles: (a) silica, (b) titania, (c) α -alumina and (d) polystyrene.
2 Each spectra has the background subtracted. Background spectra are acquired without the particle
3 present but with all other conditions identical. The trapping laser power was 15 mW from the top
4 objective and 10 mW from the lower objective. Raman laser power was 9 mW for spectra (a)-(c) and
5 6 mW for spectrum (d).



6

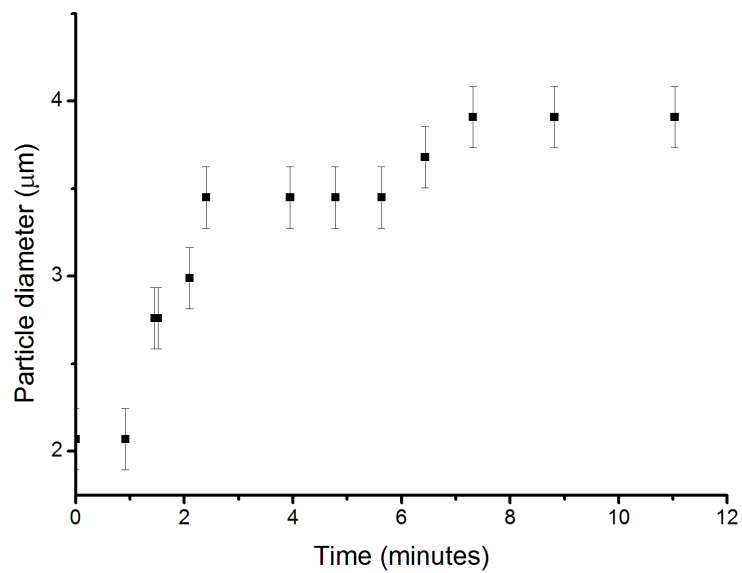
- 1 **Figure 4:** (a) Raman spectra of trapped silica particles under different relative humidity conditions.
2 The trapping cell temperature was 293.5 ± 0.1 K. Note the growth of the peaks centred at 640 and
3 1805 cm^{-1} as a function of the relative humidity. (b) Average peak area of the peak centred at 1805
4 cm^{-1} . The error bars represent the integration error. Trapping laser power was 15 mW from the top
5 objective and 10 mW from the lower objective. The Raman laser power was 6 mW.



6

1 **Figure 5:** Increase in trapped particle diameter as the initially trapped silica particle collides and
2 coagulates with sulphuric acid microdroplets. The particle diameter is determined by the optical
3 imaging camera and the images are processed using Image J software.

4



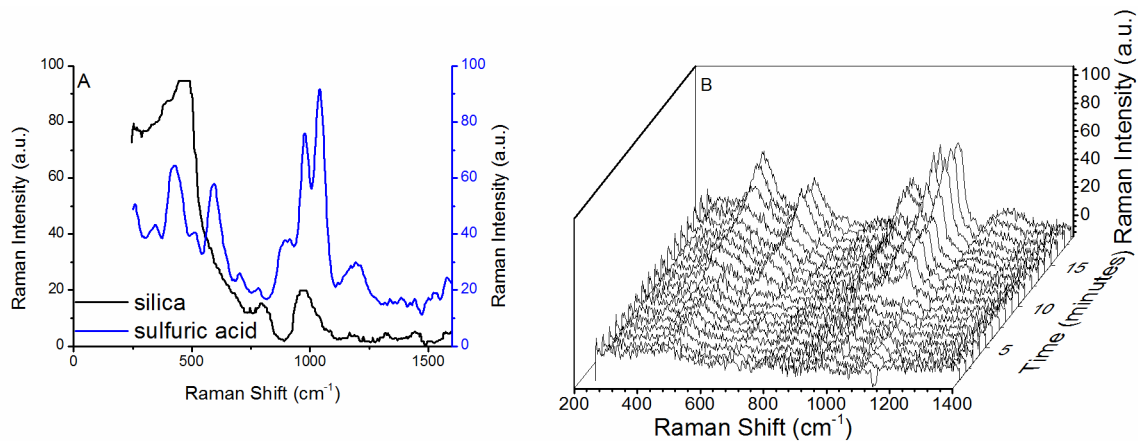
5

6

7

1 **Figure 6:** Panel A: Raman spectra of trapped a pure sulphuric acid droplet (black line) and a pure
2 silica particle (blue line). Panel B: evolution of Raman spectra of a levitated silica particle in a flow
3 of sulphuric acid microdroplets. Note the ever present silica peak at $\sim 500\text{ cm}^{-1}$, and the onset of
4 sulphuric acid spectral features at ~ 7 minutes. The trapping power was 15 mW from the top objective
5 and 10 mW from the lower objective. Raman laser power was 27 mW.

6

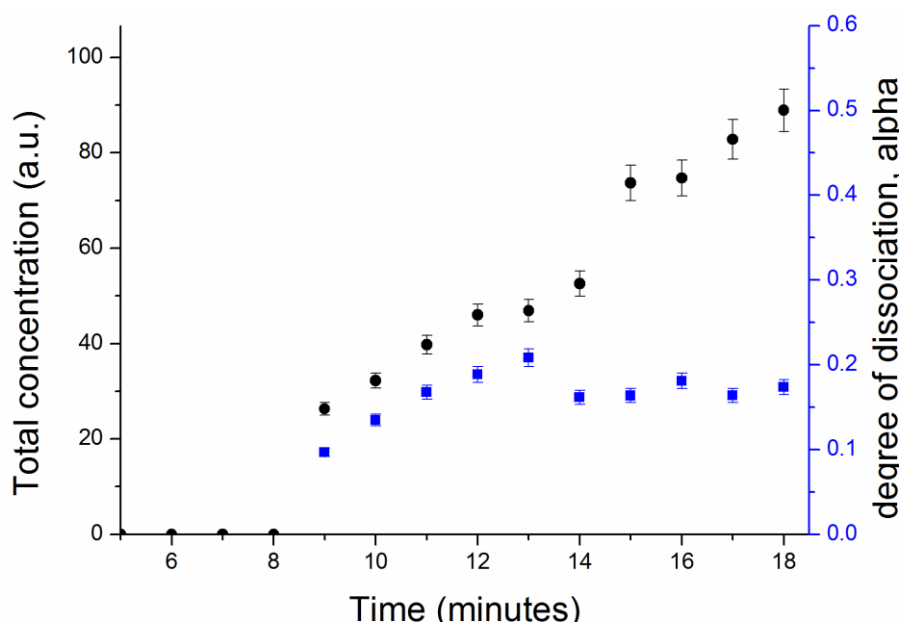


7

8

1 **Figure 7:** The relative concentration and degree of dissociation of sulphuric acid on an optically
2 levitated silica sphere in a flow of sulphuric acid microdroplets as a function of time. Left hand axis
3 and blue circles provide the relative concentration of sulphuric acid (sulphate plus bisulphate ions).
4 Right hand axis and black squares provide the degree of dissociation of the bisulphate ion (α see
5 equation E2). The trapping power was 15 mW from the top objective and 10 mW from the lower
6 objective. Raman laser power was 27 mW.

7



8

9

1 **Bibliography**

- 2 1. J. H. Seinfeld and S. N. Pandis, *Atmospheric Chemistry and Physics: From Air Pollution to*
3 *Climate Change*, Wiley-Interscience, 2nd edn., 2006.
- 4 2. M. J. Tang, P. J. Telford, F. D. Pope, L. Rkiouak, N. L. Abraham, A. T. Archibald, P. Braesicke, J.
5 A. Pyle, J. McGregor, I. M. Watson, R. A. Cox, and M. Kalberer, *Atmos Chem Phys Discuss*, 2014, **14**,
6 4421–4456.
- 7 3. M. Pradhan, M. Kalberer, P. T. Griffiths, C. F. Braban, F. D. Pope, R. A. Cox, and R. M.
8 Lambert, *Env. Sci Technol*, 2010, **44**, 1360–1365.
- 9 4. P. S. J. Matthews, M. T. Baeza-Romero, L. K. Whalley, and D. E. Heard, *Atmos Chem Phys*
10 *Discuss*, 2014, **14**, 4229–4261.
- 11 5. F. D. Pope, P. Braesicke, R. G. Grainger, M. Kalberer, I. M. Watson, P. J. Davidson, and R. A.
12 Cox, *Nat. Clim. Change*, 2012, **2**, 713–719.
- 13 6. M. Che and J. C. Vedral, *Characterization of Solid Materials and Heterogeneous Catalysts:*
14 *From Structure to Surface Reactivity*, 2012.
- 15 7. S. D. Jackson and J. S. J. Hargreaves, *Metal Oxide Catalysis*, John Wiley & Sons, 2009.
- 16 8. M. D. King, K. C. Thompson, and A. D. Ward, *J. Am. Chem. Soc.*, 2004, **126**, 16710–16711.
- 17 9. F. D. Pope, H.-J. Tong, B. J. Dennis-Smith, P. T. Griffiths, S. L. Clegg, J. P. Reid, and R. A. Cox,
18 *J. Phys. Chem. A*, 2010, **114**, 10156–10165.
- 19 10. F. Priego-Capote and L. de Castro, *Trac-Trends Anal. Chem.*, 2006, **25**, 856–867.
- 20 11. U. K. Krieger, C. Marcolli, and J. P. Reid, *Chem. Soc. Rev.*, 2012, **41**, 6631–6662.
- 21 12. A. Ashkin, *Biophys. J.*, 1992, **61**, 569–582.
- 22 13. D. M. Carberry, S. H. Simpson, J. A. Grieve, Y. Wang, H. Schäfer, M. Steinhart, R. Bowman, G.
23 M. Gibson, M. J. Padgett, S. Hanna, and M. J. Miles, *Nanotechnology*, 2010, **21**, 175501.
- 24 14. P. Galajda and P. Ormos, *J. Opt. B Quantum Semiclassical Opt.*, 2002, **4**, S78.
- 25 15. P. J. Pauzauskie, A. Radenovic, E. Trepagnier, H. Shroff, P. Yang, and J. Liphardt, *Nat. Mater.*,
26 2006, **5**, 97–101.
- 27 16. R. C. Gauthier, M. Ashman, and C. P. Grover, *Appl. Opt.*, 1999, **38**, 4861–4869.
- 28 17. H. Sosa-Martínez and J. C. Gutiérrez-Vega, *J. Opt. Soc. Am. B*, 2009, **26**, 2109–2116.
- 29 18. T. Li and M. G. Raizen, *Ann. Phys.*, 2013, **525**, 281–295.
- 30 19. K. Tajiri, M. Tachikawa, and K. Nagashima, *Appl. Phys. Lett.*, 2006, **88**, 141111.
- 31 20. J. K. Nielsen, C. Maus, D. Rzesanke, and T. Leisner, *Atmos Chem Phys*, 2011, **11**, 2031–2037.

- 1 21. J. Wu, *J. Acoust. Soc. Am.*, 1991, **89**, 2140–2143.
- 2 22. A. Ashkin and J. M. Dziedzic, *Appl. Phys. Lett.*, 1971, **19**, 283–285.
- 3 23. A. Ashkin, J. M. Dziedzic, J. E. Bjorkholm, and S. Chu, *Opt. Lett.*, 1986, **11**, 288–290.
- 4 24. E. J. Davis, *Aerosol Sci. Technol.*, 1997, **26**, 212–254.
- 5 25. R. Omori, T. Kobayashi, and A. Suzuki, *Opt. Lett.*, 1997, **22**, 816–818.
- 6 26. R. J. Hopkins, L. Mitchem, A. D. Ward, and J. P. Reid, *Phys. Chem. Chem. Phys.*, 2004, **6**,
7 4924–4927.
- 8 27. M. D. King, K. C. Thompson, and A. D. Ward, *J. Am. Chem. Soc.*, 2004, **126**, 16710–16711.
- 9 28. H.-J. Tong, J. P. Reid, D. L. Bones, B. P. Luo, and U. K. Krieger, *Atmos Chem Phys*, 2011, **11**,
10 4739–4754.
- 11 29. Y. Arita, A. W. McKinley, M. Mazilu, H. Rubinsztein-Dunlop, and K. Dholakia, *Anal. Chem.*,
12 2011, **83**, 8855–8858.
- 13 30. M. D. Summers, D. R. Burnham, and D. McGloin, *Opt. Express*, 2008, **16**, 7739–7747.
- 14 31. G. G. Hoffmann, E. Lentz, and B. Schrader, *Rev. Sci. Instrum.*, 1993, **64**, 823–824.
- 15 32. T. Li, S. Kheifets, and M. G. Raizen, *Nat. Phys.*, 2011, **7**, 527–530.
- 16 33. T. Li and M. G. Raizen, *Brownian motion at short time scales*, 2012.
- 17 34. T. Li, S. Kheifets, D. Medellin, and M. G. Raizen, *Science*, 2010, **328**, 1673–1675.
- 18 35. T. B. Lindballe, M. V. Kristensen, A. P. Kylling, D. Z. Palima, J. Glüeckstad, S. R. Keiding, and H.
19 Stapelfeldt, *J. Eur. Opt. Soc. Rapid Publ.*, 2011, **6**.
- 20 36. P. Kraikivski, B. Pouligny, and R. Dimova, *Rev. Sci. Instrum.*, 2006, **77**, 113703.
- 21 37. C. A. McNamara, M. J. Dixon, and M. Bradley, *Chem. Rev.*, 2002, **102**, 3275–3300.
- 22 38. D. V. Petrov, *J. Opt. Pure Appl. Opt.*, 2007, **9**, S139.
- 23 39. P. McMillan, *Am. Mineral.*, 1984, **69**, 622–644.
- 24 40. A. M. Efimov and V. G. Pogareva, *Chem. Geol.*, 2006, **229**, 198–217.
- 25 41. L. S. Hsu and C. Y. She, *Opt. Lett.*, 1985, **10**, 638–640.
- 26 42. L. S. Hsu, R. Rujkorakarn, J. R. Sites, and C. Y. She, *J. Appl. Phys.*, 1986, **59**, 3475–3480.
- 27 43. F. D. Hardcastle, H. Ishihara, R. Sharma, and A. S. Biris, *J. Mater. Chem.*, 2011, **21**, 6337.
- 28 44. S. P. S. Porto and R. S. Krishnan, *J. Chem. Phys.*, 1967, **47**, 1009–1012.
- 29 45. J. T. Klopogge, H. D. Ruan, and R. L. Frost, *J. Mater. Sci.*, 2002, **37**, 1121–1129.

- 1 46. A. Palm, *J. Phys. Chem.*, 1951, **55**, 1320–1324.
- 2 47. R. Bowman, A. Jesacher, G. Thalhammer, G. Gibson, M. Ritsch-Marte, and M. Padgett, *Opt.*
3 *Express*, 2011, **19**, 9908–9914.
- 4 48. O. R. Hunt, A. D. Ward, and M. D. King, *RSC Adv.*, 2013.
- 5 49. D. A. Knopf, B. P. Luo, U. K. Krieger, and T. Koop, *J. Phys. Chem. A*, 2003, **107**, 4322–4332.
- 6 50. J. F. Lübben, C. Mund, B. Schrader, and R. Zellner, *J. Mol. Struct.*, 1999, **480–481**, 311–316.
- 7 51. F. Fan, Z. Feng, and C. Li, in *Characterization of Solid Materials and Heterogeneous Catalysts*,
8 eds. M. Che and J. C. Védrine, Wiley-VCH Verlag GmbH & Co. KGaA, 2012, pp. 49–87.
- 9 52. H. F. Hameka and J. O. Jensen, *J. Mol. Struct. THEOCHEM*, 1995, **331**, 203–214.
- 10 53. M. Tasumi, T. Urano, and M. Nakata, *J. Mol. Struct.*, 1986, **146**, 383–396.
- 11 54. C. La Lau and R. G. Snyder, *Spectrochim. Acta Part Mol. Spectrosc.*, 1971, **27**, 2073–2088.
- 12 55. N. Fuson, C. Garrigou-Lagrange, and M. L. Josien, *Spectrochim. Acta*, 1960, **16**, 106–127.
- 13 56. W. H. Wright, G. J. Sonek, and M. W. Berns, *Appl. Phys. Lett.*, 1993, **63**, 715–717.
- 14 57. M. D. Summers, D. R. Burnham, and D. McGloin, *Opt. Express*, 2008, **16**, 7739.
- 15 58. K. M. Davis and M. Tomozawa, *J. Non-Cryst. Solids*, 1995, **185**, 203–220.
- 16 59. G. Buscarino, G. Vaccaro, S. Agnello, and F. M. Gelardi, *J. Non-Cryst. Solids*, 2009, **355**, 1092–
17 1094.
- 18 60. G. Buscarino, V. Ardizzone, G. Vaccaro, and F. M. Gelardi, *J. Non-Cryst. Solids*, 2011, **357**,
19 1866–1870.
- 20 61. M. Dračínský, L. Benda, and P. Bouř, *Chem. Phys. Lett.*, 2011, **512**, 54–59.
- 21 62. S. Solomon, *Rev. Geophys.*, 1999, **37**, 275–316.
- 22 63. G. D. Yadav and J. J. Nair, *Microporous Mesoporous Mater.*, 1999, **33**, 1–48.
- 23 64. J. M. Riego, Z. Sedin, J. Zaldívar, N. C. Marziano, and C. Tortato, *Tetrahedron Lett.*, 1996, **37**,
24 513–516.
- 25 65. C. E. Lund Myhre, D. H. Christensen, F. M. Nicolaisen, and C. J. Nielsen, *J. Phys. Chem. A*,
26 2003, **107**, 1979–1991.
- 27 66. C. Mund and R. Zellner, *Chem Phys Chem*, 2003, **4**, 638–645.
- 28 67. B. S. W. Dawson, D. E. Irish, and G. E. Toogood, *J. Phys. Chem.*, 1986, **90**, 334–341.
- 29 68. G. M. Brown and G. A. Hope, *J. Electroanal. Chem.*, 1995, **382**, 179–182.
- 30 69. A. S. Wexler and S. L. Clegg, *J. Geophys. Res. Atmospheres*, 2002, **107**, ACH 14–1.

1

Physical Chemistry Chemical Physics Accepted Manuscript